4 Experimental evaluation of catalyst layers with bimodal pore structure for Fischer–Tropsch synthesis

With permission from Elsevier, reproduced from:
H. Becker, R. Güttel, T. Turek
Catal. Today, **2016**, 275, 155–163
DOI: 10.1016/j.cattod.2015.11.009

4.1 Abstract

As catalyst pores are typically filled with liquid, long-chained hydrocarbons during low-temperature Fischer–Tropsch synthesis internal mass transport limitations can impede conversion rate and C_{5+} selectivity. Utilization of transport pores may improve reactant diffusion and thereby reduce these negative effects. In this work preparation, characterization and experimental testing of $CoRe/Al_2O_3$ catalyst layers, with and without transport pores, of different thickness is presented. All prepared layers with thicknesses in the range from 50 to 600 µm exhibit similar cobalt crystallite sizes of 8.7 nm irrespective of the presence of transport pores. Experimental results showed an increase in methane selectivity from 10 to 40% and a drop of C_{5+} selectivity from 80 to 42% with increasing diffusion length. These negative effects could be retarded by use of transport pores. The highest CO conversion was achieved for layers of about 140 µm thickness exhibiting 50–70% higher values than obtained with the thinnest layers (50–60 µm). This trend also holds for layers with transport pores, but the use of additional pores did not result in a significant improvement of conversion and space time yield. Nonetheless, on a catalyst mass basis transport pores lead to a benefit in productivity of 25–50%.

4.2 Keywords

FTS, transport pores, mass transport limitation, cobalt, productivity, diffusion length

4.3 Introduction

Fischer-Tropsch (FT) synthesis is a viable process for the conversion of syngas to hydrocarbons that can be used for the production of e.g. diesel fuels. To ensure an efficient process, a high selectivity towards long-chained hydrocarbons is inevitable. Thus the low-temperature process on cobalt-based catalysts is typically used for this purpose [1]. Since under reaction conditions, some products remain in the liquid phase, the catalyst pores are generally assumed to be filled with liquid that strongly affects the diffusion of the reactants. Especially in fixed bed reactors, where larger particles are usually employed to maintain a low pressure drop [2], diffusion limitations may restrict the productivity and negatively affect the selectivity. Post et al. [3] have shown that severe diffusion limitations limit the rate of carbon monoxide conversion in a fixed bed reactor with catalyst on different supports. Washcoated monoliths utilizing a $CoRe/Al_2O_3$ catalyst have been evaluated by different groups [4-7], which showed a negative influence of too high diffusion lengths on activity and product selectivity but also some effects of external mass transport [8, 9]. A critical thickness of about 50 µm was found to be the upper limit from which on negative effects of pore diffusion can appear. The group of Iglesia [10-12] has investigated various FT catalysts in fixed bed reactors and could show that diffusion effects do not only negatively affect activity and selectivity, but may also have a positive influence on selectivities due to increased readsorption and subsequent secondary growing of α-olefinic products. However, these positive effects are only marginal, especially for higher diffusion lengths, and thus different approaches have been suggested to overcome these diffusion limitations. The use of egg-shell catalysts, where only a thin outer layer of a larger catalyst particle is active, reduces diffusion limitations [11, 13, 14]. But as the core of the particles is not catalytically active, a significant fraction of the reactor is filled with inert material which lowers the reactor productivity. Hence the structure of the catalyst can be seen as part of the problem [15, 16] and an alternative approach aims at modifying the pore structure of the catalyst. Typically small pores are required to confine the available space for cobalt and cobalt oxide crystallites during catalyst preparation and to obtain a high metallic surface area of the catalyst [17, 18]. As the optimum cobalt crystallite size is about 5 to 6 nm [19, 20] catalyst support materials exhibit pore diameters with similar size. In this pore size range, the diffusion of the reactants in liquid-filled pores can be seriously hindered. Although theoretical predictions for ideal structures and empirical equations mostly predict a tortuosity between one and three [21], some experimental results show much higher values of up to 40 [22]. A possible reason for this observation

is a restricted diffusion within narrow pores, where the size of the solute is in the same order of magnitude as the pore diameter [23-26]. This phenomenon is similar to the well-known Knudsen diffusion in the gas phase and the dependence of the diffusivity on the pore size is motivation for the use of catalysts with bimodal pore structure. Such catalysts take advantage of narrow mesopores or micropores to obtain a high activity and exhibit a certain volume fraction of macropores to improve mass transport. For simple first-order kinetics and one- to two-dimensional problems simulation and optimization results of the group of Coppens [27-30] have clearly shown, that an ideal volume fraction of transport pores has to be found in order to enhance mass transport on the one hand and to preserve the amount of active phase on the other hand. For high Thiele moduli, this optimized volume fraction remains constant at a value of 0.5 as long as the transport pores are sufficiently small. For this case, a homogenous distribution of transport pores was shown to be almost as beneficial as an optimized spatial distribution of pores. An experimental study from the group of Tsubaki [31, 32] of impregnated macroporous, microporous and bimodal catalyst supports has revealed that bimodal catalyst combine an increased activity with high selectivity towards long chained products. Further evaluation of this experimental data with a process model supports the authors assumption of improved mass transport as a result of utilizing transport pores [33]. Despite these promising results, it remains unclear if a real enhancement of mass transport could be achieved. In this study, only one catalyst sieve fraction with diameters below 149 µm was used; hence, the effective diffusion length was not clearly defined. Furthermore, the used catalysts were differently prepared and thus, the effects of the support structure and material on intrinsic activity and selectivity cannot be ruled out. As the pore size is an important parameter during impregnation, drying and calcination [34] preparation of bimodal catalysts can increase reducibility but also cobalt oxide crystallite size [35]. For macroporous structured catalysts, Phan et al. [36] were able to show effects of the bimodal catalyst support itself on intrinsic selectivity and activity without even considering mass transport. Evaluation of catalysts prepared from conventional supports with different pore size and comparison to a bimodal catalyst revealed a positive effect of increasing support pore size on product selectivity. However, a rather ambiguous effect on productivity regarding pore size and use of transport pores was found [37]. Recent work from Wang, et al. [38] compares different bimodal catalysts with variable mesopore size but constant micropore size finding the highest conversion at the biggest mesopore size but the highest C_{5+} selectivity for median mesopores. Despite the importance of diffusion length on diffusional limitations, no experimental

work has already reported the effects of variation of transport pore fraction and diffusion length.

In previous work based on simulation [39, 40] utilizing empirical equations [41, 42] we have shown that insertion of transport pores gives rise to enhanced reactor productivity provided that both, diffusion length and transport pore fraction are optimized. Moreover, the resulting optimum strongly depends on the effective diffusion within transport pores and catalyst pores. Thus, evaluation of mass transport effects of transport pores requires a comparable, well-defined catalyst with variable diffusion length and transport pore fraction. In this work, we present a method for preparation of catalyst layers with adjustable thickness, with and without transport pores, which were prepared from the same catalyst base powder to investigate diffusion limitations during FT reaction.

4.4 Experimental

4.4.1 Catalyst preparation

The catalyst powder used in this study contains 20% Cobalt and 1% Rhenium in the reduced state and was prepared by impregnation of a γ-Al_2O_3 support (Puralox UF5/230, 5 µm, Sasol) as described elsewhere [8]. For the preparation of the catalyst layers, a suspension of the base powder was sprayed on stainless steel plates (25 mm × 50 mm × 0.5 mm) using an airbrush (Evolution SOLO, Harder & Steenbeck) with a nozzle of 0.4 mm in diameter operated at 2 bar gauge pressure of nitrogen. The suspension consisted of a mixture of 10 g of catalyst, 7.0 g of colloidal binder (pseudo-boehmite, 20 wt%, 50 nm, pH 7, Alfa Aesar) and 4.0 g polyethylene glycol (20,000 g/mol, Fluka) in 29 g of deionized water and 7.0 g of 2-propanol. The mixture was vigorously stirred and ultrasonically dispersed before spraying the suspension on the metal plates heated to 90 °C. To adjust the layer thickness the number of spraying runs was used as a rough estimate and checked by measuring the gain in mass. The still wet layers were then either compacted with a pressure of 1.5 t/cm² for 1 min in a laboratory press (Labopress P200S, Vogt) or the layers were directly heat treated. Both types of layers, denoted as compacted or uncompacted, were then heated in air with a rate of 2 K/min to a temperature of 400 °C, which was kept for 4 h. After cooling to below 50 °C, the layers were removed from the oven and used for characterization. The average thickness of each layer sample was measured using a thickness dial gauge (Käfer) at 6 points, allowing to keep the layers intact. Layers with a thickness ranging from 60 to 600 µm were

prepared. Each layer thickness was prepared at least two times ensuring that sufficient sample mass was available for analysis and Fischer-Tropsch reaction experiments.

4.4.2 Fischer-Tropsch experiments

Catalyst testing was conducted similar to previous work [2, 43, 44]. The catalysts layers were placed in an aluminium inlay with a channel height of 1.5 mm and a width of 25 mm. The catalyst layers were located on one side of the inlet leaving a void channel thickness of about 0.5 to 1.0 mm depending on the layer thickness. To ensure good contact to the heated wall of the reactor, an inert carbon felt (GFD2.5 EA, SGL Carbon) was placed above the catalyst layer. The carbon felt is highly porous even after compaction and did not lead to a measurable pressure drop in the channel during the reaction. The catalysts were reduced in the reactor with a mass-specific flow of pure hydrogen of 10 $L_{STP}/(h\,g_{cat})$ starting at a temperature of 120 °C. Subsequently, the temperature was increased up to 350 °C with a rate of 50 K/h and kept there for 16 h. After reduction and cooling down to 150 °C the reaction was started. The reactor was pressurized to 2.1 MPa with a syngas flow proportional to a GHSV of 5000 $m^3_{SG}/(m^3_{Cat}$ h) and a H_2/CO ratio of 2.0. Argon was used as internal standard and was dosed together with carbon monoxide directly from the gas cylinder (10% argon in carbon monoxide). During activation the temperature was increased up to 190 °C every 12 h in steps of 10 K. After this procedure the system was given time, typically 24 to 48 h, to reach steady-state at each temperature before the temperature was increased again in steps of 10 K to a maximum of 240 °C. During synthesis water and liquid hydrocarbons were separated in a cold and a hot trap, operating at 0° and 120 °C, respectively. Gaseous products were analyzed in a Varian GC-450 equipped with an FID, for hydrocarbon analysis, and a TCD detector channel for the permanent gases. Carbon monoxide conversion, X_{CO}, and methane selectivity, S_{C1}, were calculated as reported elsewhere [44]. The C_{5+} selectivity, S_{C5+}, was calculated on a carbon basis. In accordance with equation (4.1) and (4.2) space time yield, STY, and mass-specific productivity, MTY, were estimated using the H_2/CO ratio, the apparent density, ϱ_{app}, of the catalyst and the molar volume at standard conditions, v_{STP}.

$$STY = \frac{X_{CO} \cdot S_{C5+} \cdot GHSV}{(1 + H_2/CO) \cdot v_{STP}} \tag{4.1}$$

$$MTY = \frac{STY}{\rho_{app}} \tag{4.2}$$

4.4.3 Temperature-programmed reduction

For the temperature-programmed reduction (TPR), the powder catalyst and broken pieces of catalyst layers were analyzed with a BelCat M (Bel, Japan) device. About 15 mg of sample was heated prior to the analysis in an argon flow of 30 mL/min to a temperature of 120 °C with a dwell time of 30 min. After that, the temperature was decreased to 50 °C before a gas mixture of 10% hydrogen in argon was applied with a flow rate of 15 mL/min. Then the temperature was ramped with a rate of 10 K/min to a maximum of 950 °C and kept for 15 min. The effluent gas was analyzed with a TCD after passing a water trap filled with a molecular sieve. Integration of the signal allows measuring the amount of hydrogen consumed. For calibration of the TPR experiments, nickel(II) oxide was used (Puratronic®, 99.998% (metals basis), Alfar Aesar). Assuming that only Co_3O_4 is reduced, the total amount of cobalt can be determined from the uptake of hydrogen.

4.4.4 Nitrogen physisorption

Nitrogen physisorption was conducted with an ASAP 2020 (Micromeritics) device to quantify the size and the specific volume of the mesopores of the catalyst. Typically a sample mass of 70 to 100 mg was degassed at a temperature of 250 °C for 2 h prior to analysis in liquid nitrogen. During the measurements, 180 data points for adsorption and desorption were collected. The pore size distribution was calculated according to the BJH method and the total pore volume, v_{Cat}, was determined from the quantity adsorbed at a relative pressure of 0.99.

4.4.5 Mercury intrusion

The size and the volume of the transport pores were determined with mercury intrusion measurements. A typical sample mass of 70 to 100 mg was analysed in a Pascal 140 device first and then in a Pascal 440 (both from Porotec) system. The specific pore volume was divided into three sections. The first section with all pores below 100 nm corresponds to the pore volume estimated with N_2 physisorption. The second one, v_{TP}, comprises pores between 100 nm and 5 µm and represents the volume of transport pores. The last section, with pores above 5 µm, provides only information about pores that are formed during the removal of the catalyst from the steel plate and is thus not further evaluated.

4.4.6 Roughness and texture

The roughness of the catalyst layer surfaces was measured with a Tencor P1 profilometer on 5 different positions at each layer. During measurement, low-frequency waviness was already processed and subtracted from the height signal. Further analysis of the catalyst structure was conducted using a scanning electron microscope (DSM 982 Gemini, Zeiss) after sputtering with platinum.

4.4.7 Density and porosities

The apparent density, ϱ_{app}, can be simply calculated via the layer mass and layer thickness. For porosity calculations also the skeleton density is required, which was measured with a helium pycnometer (pycnomatic, Porotec). As this method requires quite high masses of about 5 to 10 g to be reliable, only the catalyst powder and a sample of the dried and heated binder could provide enough mass for the measurement. The skeleton density of the layers was calculated according to the density of binder and catalyst powder and their mass fraction in the layers. The catalyst porosity, ε_{Cat}, was calculated according to equation (4.3), based on the skeleton density, ϱ_s, and the pore volume obtained from N_2 physisorption, v_{Cat}. equation (4.4) additionally uses the pore volume from mercury intrusion, v_{TP}, to determine the transport pore porosity. Alternatively, the transport porosity can be calculated with help of the apparent density (equation (4.5)).

$$\varepsilon_{Cat} = \frac{v_{Cat}}{v_{Cat} + \frac{1}{\rho_s}} \tag{4.3}$$

$$\varepsilon_{TP} = \frac{v_{TP}}{v_{TP} + v_{Cat} + \frac{1}{\rho_s}} \tag{4.4}$$

$$\varepsilon_{TP} = 1 - \left(\frac{1}{\rho_s} - v_{Cat}\right)\rho_{app} \tag{4.5}$$

4.4.8 Chemisorption and oxygen titration

The cobalt dispersion and crystallite size were measured by adsorption of H_2 and subsequent oxygen titration using the volumetric adsorption method (3Flex, Micromeritics). For that purpose ca. 70 mg of the sample were reduced under a mass-

specific hydrogen flow of 16.6 $mL_{STP}/(min\ g_{Cat})$ for 16 h at 350 °C, followed by 30 min evacuation at this temperature and chemisorption of pure H_2 at 50 °C. After chemisorption, the sample was again evacuated and heated to 400 °C before oxygen titration was conducted. Assuming that at this temperature the oxygen uptake leads to Co_3O_4 only [45] the degree of reduction, *DOR*, the corrected dispersion, D_{corr}, and the crystallite size [18], d_{Co}, can be calculated as follows:

$$DOR = \frac{n_{Co,reduced}}{n_{Co,total}} = 2\frac{n_{O_2}}{n_{H_2,TPR}} \tag{4.6}$$

$$D_{corr} = \frac{n_{Co,surface}}{n_{Co,reduced}} = \frac{4}{3}\frac{n_{H_2,Chemi}}{n_{O_2}} \tag{4.7}$$

$$d_{Co} = \frac{96\ nm}{\frac{D_{corr}}{[\%]}} \tag{4.8}$$

4.5 Results and discussion

4.5.1 Preparation results and ex-situ characterization

After spraying, drying and calcination mechanically stable layers were obtained. The layer thickness was adjusted via the deposited mass on the metallic support. The measured thicknesses for all prepared layers range from 63 µm to slightly above 600 µm. Obviously, the mass of compacted layers with the same thickness as uncompacted layers is higher throughout the entire thickness range (figure (4.1), left). For both types of layers, the linear correlation between thickness and mass leads to a positive y-axis offset. This offset is with a value of 26.6 µm significantly higher for uncompacted layers than for the compacted layers, where only a value of 15.9 µm was found. This is a result of the surface roughness of the layers. As the virginal surface of the uncompacted layers directly originates from the random deposition of catalyst particles during spraying, its roughness is much higher than for the compacted layers, which is clearly visible in the profile plot (figure (4.1), right). To avoid the high roughness mimicking a lower apparent density of the layers and thereby overestimating the transport pore fraction, the layer thickness was corrected by one half of the offset estimated in figure (4.1), left.

Pore size and volume were analysed via porosimetry measurements and nitrogen physisorption. The pore size distribution from the BJH method shows no significant influence of the preparation on the original mesopores inside the catalyst particles (figure (4.2), top, left). All three peaks show a quite sharp maximum at 6 nm at comparable height. The only difference is a small shoulder between 10 and 40 nm with a maximum at 16 nm for the catalyst layers. The shoulder is slightly more emphasized for the uncompacted layers and can be attributed to the addition of binder. Consequently, the pores inside the catalyst remain mainly unaffected during layer preparation. This can also be seen from the porosimetry results where the peak of the mesopores appears at similar pore size, again with the characteristic shoulder (figure (4.2), top, right). For the catalyst powder and the uncompacted catalyst layer, a second peak appears in the range of about 0.1 to 5 µm. Any appearing residual pore volume at larger pore sizes is negligible since it results from cracks in the samples and gaps between the sample pieces introduced during removal of the layer from the metallic carrier. For the uncompacted layer, the maximum of the second peak lies at 0.4 µm, whereas for the powder the maximum appears at 0.7 µm. Additionally, the pore volume of this peak for the catalyst powder is significantly larger than for the uncompressed layer. The compacted layer features no such peak at all. Hence, this peak can be explained as a result of the gaps between the packing of spherical catalyst particles. Although the catalyst powder consists of loose, not connected particles, a dense packing is enforced due to the severe

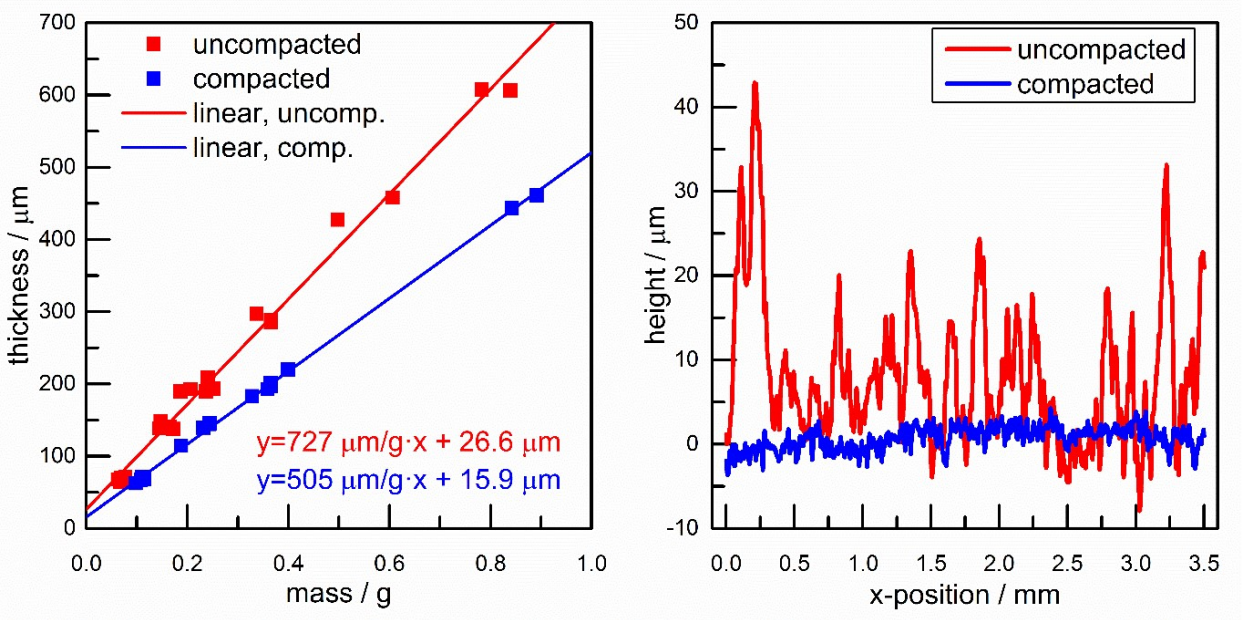

Figure 4.1: Measured thickness of compacted and uncompacted catalyst layers as a function of catalyst mass (left); height profile of a compacted and an uncompacted layer with a thickness of 140 to 145 µm (right).

applied pressure during mercury intrusion measurements. Addition of binder for preparation of layers fills these gaps between the particles to some extent and reduces pore volume and pore size. For the compacted layers, the gaps become so small that the binder completely fills this volume. SEM images of layer fragments support this assumption (figure (4.2), bottom) as they show a more open structure and less compressed binder agglomerates from samples without compaction compared to samples after compaction. Thus, the pores between 0.1 and 5 µm are denoted as transport pores. In addition to the specific pore volume and pore sizes, also the apparent density can be used for estimation of the transport pore fraction. This density is based on the catalyst mass per area of the layer (25 mm × 50 mm) and the layer thickness. Figure 4.3 (top)

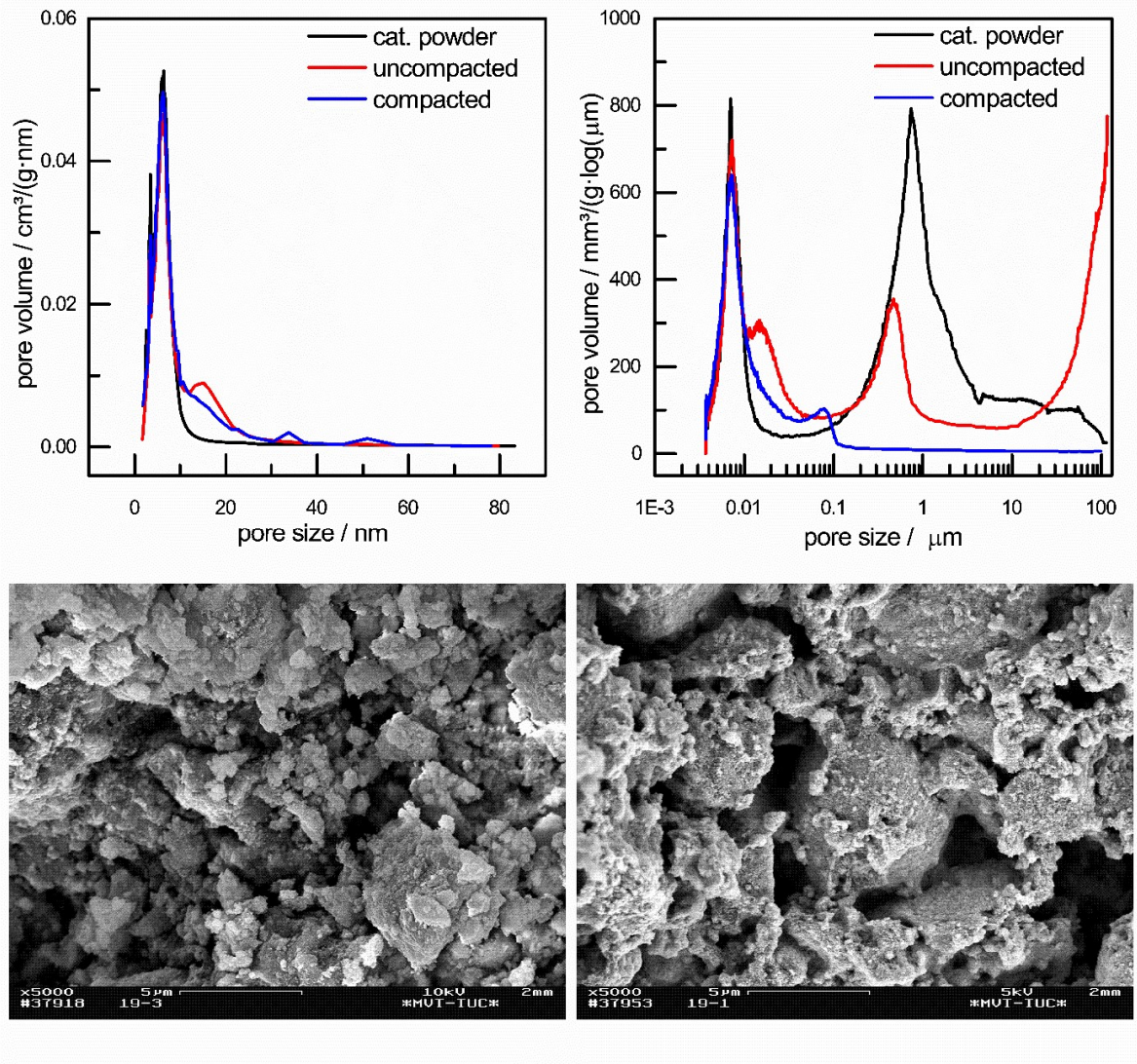

Figure 4.2: Pore size distribution from nitrogen desorption (top, left) and from mercury porosimetry (top, right) of powder catalyst, compacted and uncompacted layer pieces; SEM image of catalyst layer pieces of compacted (bottom, left) and uncompacted (bottom, right) layers.

displays these values for all prepared layers. The densities for the uncompacted layers are clearly below the values of the compacted layers with a more intense scattering for the uncompacted ones, possibly as a result of the higher surface roughness. Nonetheless, the values are quite

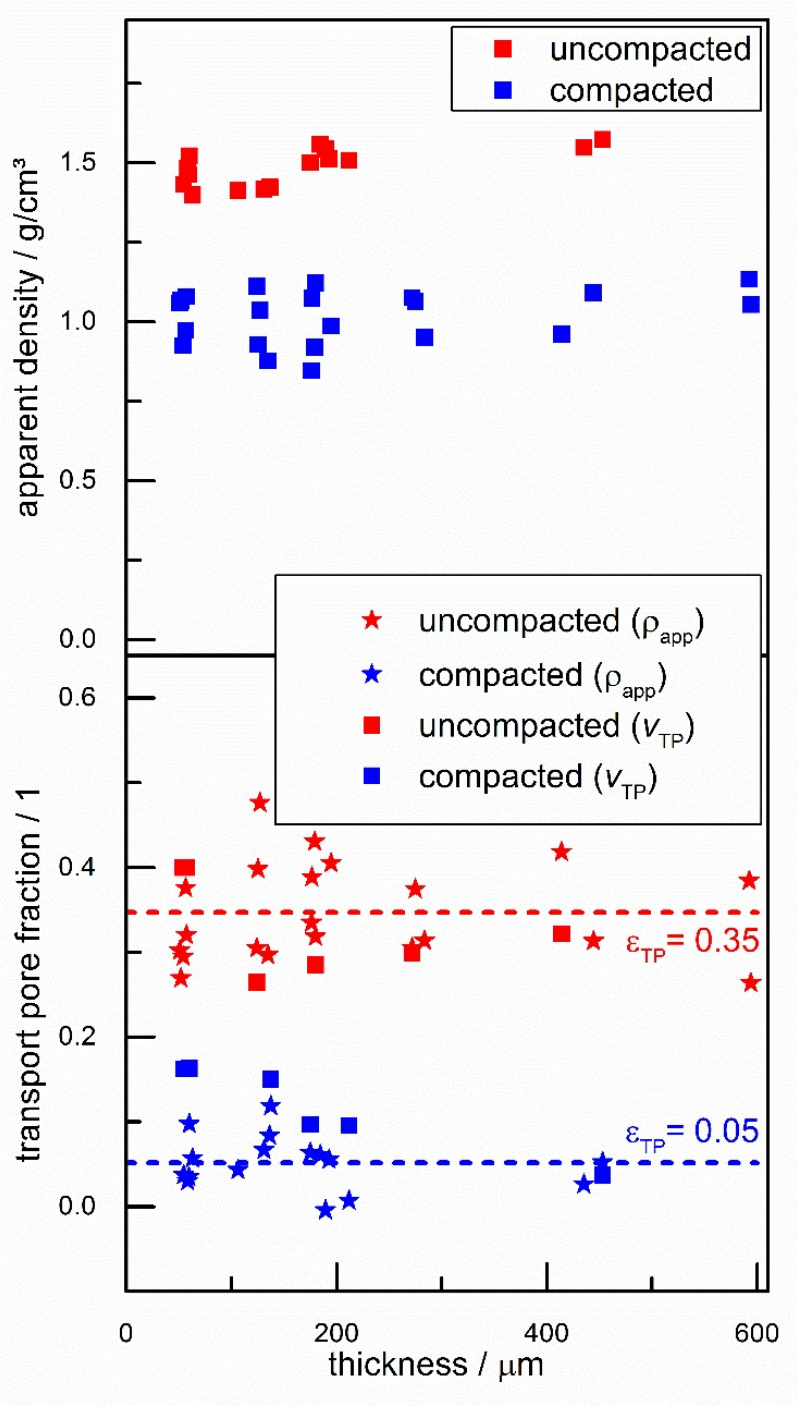

Figure 4.3: Apparent density of catalyst layers as a function of corrected layer thickness (top); transport pore fraction from mercury porosimetry (equation (4.4)) and from apparent layer density (equation. (4.5)) as a function of corrected layer thickness (bottom).

constant over the entire thickness span. Despite this almost thickness-independent density, the resulting transport pore fraction is still slightly varying as a function of the thickness (figure (4.3) bottom). For both calculation methods (equation (4.4) and equation (4.5)) in general, similar tendencies can be found, although mercury intrusion provides rather low values for the uncompacted and higher values for compacted layers. Typically, thicker catalyst layers exhibit lower transport porosities than thin layers. This can result from the roughness of the surface and the stochastic packing of particles during deposition, especially for the not compressed layers. But also, the transport pore fraction of compressed layers can be influenced by the thickness as during compaction a dense packing of spherical catalyst particles is enforced. This particle packing can only be ideally dense if the dimension of the particles is small compared to the dimension of the packing. However, the transport porosity mainly lies in a range from 0.3 to 0.4 for the not compressed layers and between 0.0 and 0.15 for the compressed layers. On average the compaction leads to a transport porosity of about 0.05, while without compaction the transport porosity is about 0.35. Thus, the described preparation method allows for variation of the layer thickness and is also capable of producing catalyst layers without and with transport pores of a size, which is small enough to ensure a homogeneous distribution of these pores.

To ensure that all catalyst layers exhibit the same activity, hydrogen chemisorption, oxygen titration and temperature-programmed reduction were conducted (table (4.1)). Despite small variations in hydrogen uptake during reduction and one outlier even exceeding the uptake of the base powder, the highest hydrogen uptake during chemisorption was achieved by the base powder, as expected. Some variation in the oxygen uptake leads to a DOR ranging from 72% to 88% with the value of the base powder of 82% almost exactly matching the average. The resulting dispersion and cobalt crystallite size are astonishingly constant for all characterized layers. The crystallite size is with 8.7 nm on average only 5.5% larger than for the base powder which reveals that only little sintering occurred during the repeated heat treatment for layer preparation. Thus, the developed preparation method of the catalyst layers should conserve the original activity.

Table 4.1: Gas uptakes and derived characteristic parameters for compacted and uncompacted catalyst layers.

	thickness	$n_{H_2,TPR}$	$n_{H_2,Chemi}$	n_{O_2}	DOR	D_{corr}	d_{Co}
	µm	µmol/ g	µmol/ g	µmol/ g	%	%	nm
cat. powder	-	3971	142.9	1635	82	11.7	8.2
uncompacted	138	3661	118.2	1412	77	11.2	8.6
uncompacted	193	3569	124.4	1502	84	11.0	8.7
uncompacted	427	3754	135.3	1651	88	10.9	8.8
uncompacted	68	4186	122.6	1509	72	10.8	8.9
compacted	254	3535	127.1	1547	88	11.0	8.8
compacted	71	3560	122.2	1484	83	11.0	8.7
compacted	145	3684	121.7	1479	80	11.0	8.7
compacted	461	3641	127.5	1553	85	10.9	8.8

4.5.2 Experimental Fischer-Tropsch performance

For experimental evaluation, five uncompacted and four compacted layers were used, creating four pairs with comparable layer thicknesses of both types and one additional layer of the uncompacted type. For the sake of simplification, only results obtained at three temperatures (200 °C, 220 °C and 240 °C) are depicted as a function of layer thickness (figure (4.4)). The carbon monoxide conversion exhibits a similar profile for all three temperatures, where conversion generally increases with temperature and the compacted layers achieve higher conversions than the uncompacted layers of the same thickness. Only the thinnest layers at maximum temperature deviate from this trend. Interestingly, for both types of layers, the maximum of conversion in each line does not appear for the thinnest layers but for layers with a thickness of about 140 µm. Only above this point, a further increase of layer thickness leads to the expected decline in conversion. The appearance of a maximum in conversion is not typical for diffusion limitations but can be a result of the different diffusivities of carbon monoxide and hydrogen and an inhibiting effect of carbon monoxide [41]. Since CO diffuses slower than H_2, it is depleted in thick layers to a greater extent leading to a higher consumption rate. Simulations have shown that this may cause catalyst efficiencies above 100% [39, 42]. However, the introduction of transport pores leads to interesting and sometimes

unexpected results. For the lowest thickness (50 µm) and the lowest temperature (200 °C) diffusion limitations should be mostly absent and thus layers with ca. 35% transport porosity should exhibit a conversion which is reduced to only 65% of the value obtained over layers without transport pores, due to the reduced apparent layer density. This is obviously not the case as at the lowest thickness the compacted layer achieves a conversion which is almost three times higher than for the uncompacted one. Furthermore, insertion of transport pores improves mass transport and thereby shifts the exploitable diffusion length to higher values which should result in a maximum appearing at higher thicknesses than for the compacted layers. For layers of several hundred micrometres in thickness also a higher conversion for the uncompacted than for the compacted layers was expected. The experimental results show this tendency only to some extent as the conversion almost levels off for thicker layers at reaction temperatures of 200 and 220 °C.

Nevertheless, the difference in reactant diffusivities also affects the product selectivity, as a high H_2/CO ratio favours hydrocarbons of shorter chain length, especially methane. This can be clearly seen from the experimental results as the methane selectivity increases from about 10% to 17% for the thinnest layers with a strong increase in the range of 150 µm to the maximum value of 28 to 40% for the thickest layers. The C_{5+} selectivity exhibits a similar trend in the opposite direction, starting at 80% and dropping towards 42% with increasing layer thickness. An increase in temperature mainly shifts the methane selectivity to higher and the C_{5+} selectivity to lower values. Only the thickest layers remain not influenced by temperature changes from 220 to 240 °C or even show decreasing methane selectivity and increasing C_{5+} selectivity. Comparing layers with and without transport pores the thickest and the thinnest layers exhibit almost similar selectivities. In the medium thickness range, uncompacted layers typically exhibit a higher C_{5+} selectivity and lower methane selectivity. Only at 240 °C, no significant influence of transport pores can be observed. Thus, insertion of transport pores retards the negative selectivity change with increasing layer thickness allowing a more efficient production of long-chained hydrocarbons with increased diffusion length. On the one hand side, this can be attributed to the increased volume fraction available for diffusion and thereby improving the mass transport. But on the other hand side also the amount of catalyst, which is present in a certain volume of the layer, is decreased and tempers the appearance of transport limitations.

Combining conversion and C_{5+} selectivity in the space time yield, STY, it is obvious that insertion of transport pores does not lead to an improvement of reactor productivity since the STY for the compacted layers is always higher than the corresponding value

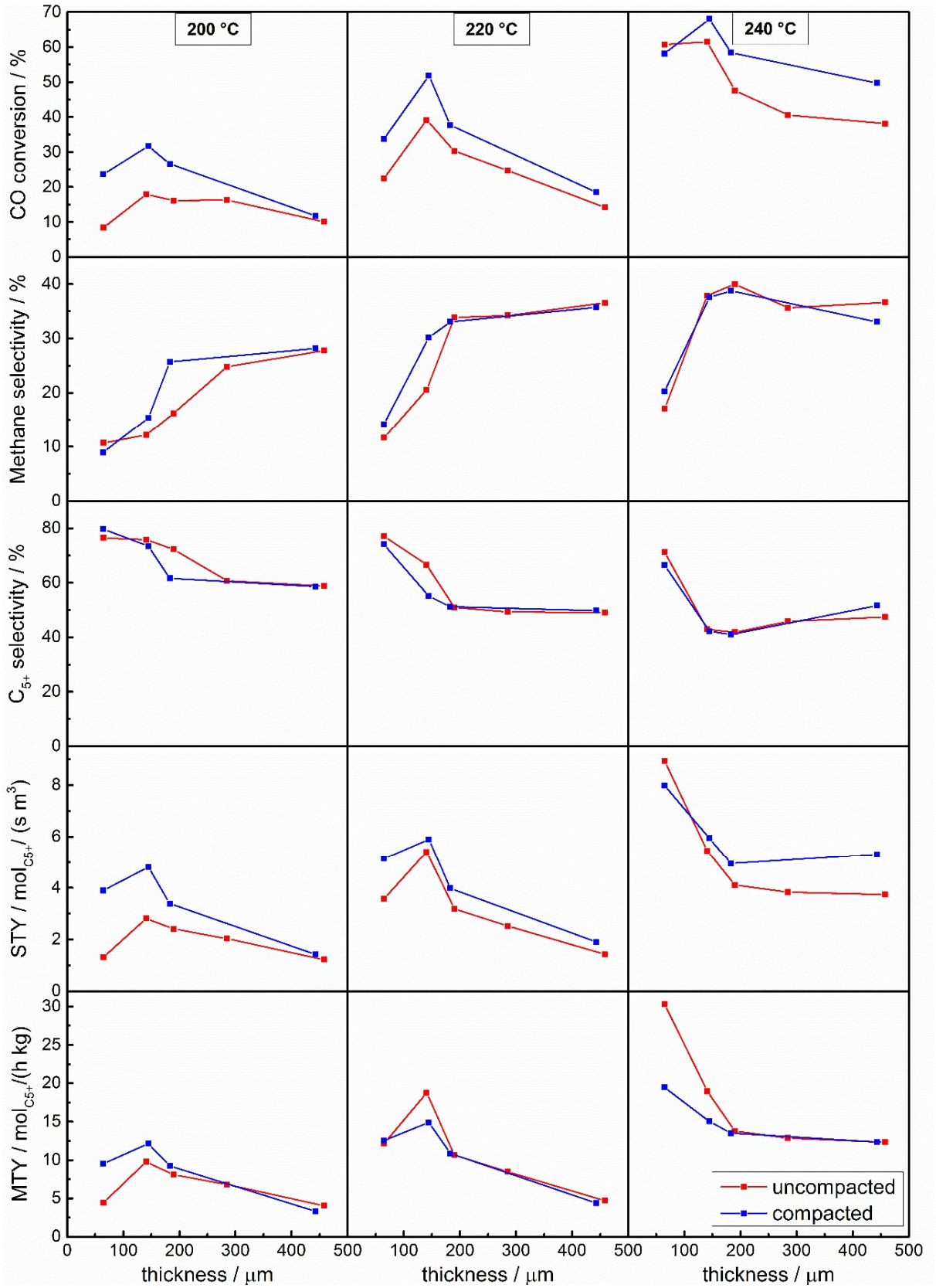

Figure 4.4: CO Conversion, methane selectivity, C_{5+} selectivity, STY and mass-specific STY (MTY) for compacted and uncompacted layers as a function of layer thickness and temperature; $p = 2.1$ MPa, $GHSV = 5000$ $m^3_{CO+H2}/(m^3_{layer}h^{-1})$, $H_2/CO = 2.0$

for the uncompacted layers. This is a result of a partially positive influence of diffusion limitations on the consumption rate and a less significant negative influence on product selectivities. Nonetheless, this does not mean that transport pores have no positive effect at all. Considering a mass-specific time yield, MTY, one can evaluate the catalyst productivity. For 220 °C and 240 °C and thicknesses from 50 to about 150 µm, insertion of transport pores allows increasing the MTY by 25 to 50% and thicker layers exhibit almost the same values for both types. A drop in productivity with increasing layer thickness as appearing at 240 °C presents the originally expected behaviour since diffusion limitations should lower the reactant concentration and thereby the effective reaction rate. However, one would expect for the absence of diffusion limitations the same mass-based productivities, which is for the thinnest investigated layers at 240 °C apparently not the case. In comparison to the values at 220 °C, one can presume, that, due to the accelerated reaction rate at higher temperatures, even the thinnest layers exhibit considerable diffusion limitations. These can explain the different mass-based productivities for the compacted and not compacted layers of 50 to 60 µm thickness.
The limited advantage through the use of transport pores can be caused by some additional phenomena that could have occurred and interfered with the experimental results. Obviously, axial concentration gradients play an important role in fixed bed reactors. Especially for high methane selectivities, the stoichiometric consumption of hydrogen per converted mole of carbon monoxide is significantly higher than 2, which is the feed ratio. Thus layers with strong diffusion limitations and resulting methane selectivities between 30 and 40% undergo a severe depletion of hydrogen in the direction of the gas flow [42]. This lowers the H_2/CO ratio to values below 2, which typically favours the production of long-chained hydrocarbons [46] and also slows down the reaction rate [41]. These effects improve catalyst efficiency and also selectivity and thereby attenuate the negative impact of diffusion limitations and impede the advantageous application of transport pores. Anyhow, this has to be evaluated in more detail by means of simulation and parameter estimation which is under current investigation in our group. But also the curiously low drop in STY for layers above 200 µm at 240 °C accompanied by decreased methane selectivity hints that some additional effect must have occurred. Although pore convection is orders of magnitudes slower than diffusive mass transport [42], the liquid products have to flow out of the pore system. If, due to strong diffusion limitations inside the catalyst layer, the selectivity towards methane and other smaller hydrocarbons were high, these products would dilute the long-chained hydrocarbons produced at the outer boundary of the layer while flowing out. This would reduce the average chain length and thereby enhance

reactants diffusivities [47] which gives rise to a lesser influence of diffusion on selectivity. This possible, but speculative influence of the product distribution on the diffusion properties can also be supported by experimental results from Kruse et al. [43]. These authors showed that a zeolite-based FT catalyst with hydroprocessing activity shifted the product distribution to lighter hydrocarbons, but lead to lower methane selectivity and higher apparent activation energy than a comparable catalyst without zeolites.
For further improvements, also the structure of the transport pores must be taken into account. As the transport pores in this work are a result of voids between the catalyst particles, no straight connection is achieved and a tortuosity considerably above unity should be the result. Hence, we propose that for major improvements, transport pores consisting of straight channels are necessary.

4.6 Conclusions

In this contribution, we present a novel method for the preparation of mechanically stable catalyst layers with and without transport pores and adjustable thickness. By using only one base powder, we kept the catalyst activity constant with almost ideal cobalt crystallite particles of 8.7 nm. The resulting thickness of the layers, (50 to 600 µm), the transport pore size (0.4 µm) and the transport pore volume fraction (0 to 40%) are in an interesting range for assessment of diffusion limitations. Furthermore, layers with a specified thickness avoid problems with ill-defined diffusion lengths in particle sieve fractions with broad particle size distributions. Moreover, layers directly placed at the reactor wall also reduce the risk of temperature gradients.
FT experiments showed a significant influence of thickness on the reaction rate and product selectivities. CO conversion benefits partially from diffusion limitations exhibiting a 50 to 70% higher conversion while increasing the thickness from about 50 to 140 µm. Only for increased thicknesses, the CO conversion drops as expected. Methane selectivity increases from 10 to 40% and C_{5+} selectivity decreases from 80 to 42% when diffusion limitations appear. Utilizing transport pores can reduce the negative effects on selectivity to some extent, but an improvement of space-time yield to C_{5+} products was not achieved. Nonetheless, the introduction of transport pores gave rise to an enhancement of the productivity per catalyst mass by 25 to 50%. The results reveal that for higher improvements in productivity also the shape of the transport pores has to be optimized, e.g. through straight transport pores with a tortuosity close to unity.

4.7 Acknowledgements

The authors thank H.C. Starck for providing us with Rhenium precursor and Sasol Germany for the alumina support material. The Deutsche Forschungsgemeinschaft is gratefully acknowledged for financial funding of this work (SPP1570, grant number TU89/9).

4.8 Notation

Latin

$n_{H2,Chemi}$	hydrogen uptake from chemisorption, $mol_{hydrogen}\ g_{catalyst}^{-1}$
$n_{H2,TPR}$	hydrogen uptake from temperature programmed reduction, $mol_{hydrogen}\ g_{catalyst}^{-1}$
n_{O2}	oxygen uptake, $mol_{oxygen}\ g_{catalyst}^{-1}$
$n_{Co,reduced}$	amount of reduced cobalt, $mol_{cobalt}\ g_{catalyst}^{-1}$
$n_{Co,surface}$	amount of cobalt on the surface, $mol_{cobalt}\ g_{catalyst}^{-1}$
$n_{Co,total}$	total amount of cobalt, $mol_{cobalt}\ g_{catalyst}^{-1}$
d_{Co}	cobalt crystallite size, m
D_{corr}	dispersion, $mol_{Co,surface}^{-1}\ mol_{Co,reduced}^{-1}$
DOR	degree of reduction, $mol_{Co,reduced}\ mol_{Co,oxidic}^{-1}$
$GHSV$	gaseous hourly space velocity, $m_{carbon\ monoxide\ +\ hydrogen}^{3}\ m_{layer}^{-3}\ h^{-1}$
MTY	mass-specific productivity to C_{5+} hydrocarbons, $mol_{C5+}\ s^{-1}\ m^{-3}$
p	pressure, Pa
S_{C5+}	C_{5+} selectivity on a carbon basis, $mol_{C5+\ carbon}\ mol_{carbon\ monoxide}^{-1}$
S_{CH4}	methane selectivity, $mol_{methane}\ mol_{carbon\ monoxide}^{-1}$
STY	volume-specific productivity to C_{5+} hydrocarbons, $mol_{C5+}\ s^{-1}\ m^{-3}$
v_{Cat}	specific pore volume of catalyst pores, $m^3\ g_{catalyst}^{-1}$
v_{STP}	molar volume of ideal gas at standard temperature and pressure, $m^3\ mol^{-1}$
v_{TP}	specific pore volume of transport pores, $m^3\ g_{catalyst}^{-1}$
X_{CO}	CO conversion, $mol_{CO\ reacted}\ mol_{CO\ fed}^{-1}$

Greek

ε_{Cat}	pore fraction inside catalyst, $m_{pore}^{3}\ m_{catalyst}^{-3}$
ε_{TP}	transport pore fraction, $m_{transport\ pore}^{3}\ m_{layer}^{-3}$
ϱ_{app}	apparent density of the catalyst, $kg_{solid}\ m_{layer}^{-3}$

ϱ_s apparent density of the catalyst, $kg_{solid}\,m_{solid}^{-3}$

4.9 References

[1] Q. Zhang, J. Kang, Y. Wang, Development of Novel Catalysts for Fischer–Tropsch Synthesis: Tuning the Product Selectivity, *ChemCatChem*, 2010, **2**, 1030-1058.

[2] C. Knobloch, R. Güttel, T. Turek, Holdup and Pressure Drop in Micro Packed-Bed Reactors for Fischer-Tropsch Synthesis, *Chem. Ing. Tech.*, 2013, **85**, 455-460.

[3] M.F.M. Post, A.C. Vanthoog, J.K. Minderhoud, S.T. Sie, Diffusion Limitations in Fischer-Tropsch Catalysts, AIChE J., 35 (1989) 1107-1114.

[4] A.M. Hilmen, E. Bergene, O.A. Lindvåg, D. Schanke, S. Eri, A. Holmen, Fischer–Tropsch synthesis on monolithic catalysts of different materials, Catal. Today, 69 (2001) 227-232.

[5] R.M. de Deugd, R.B. Chougule, M.T. Kreutzer, F.M. Meeuse, J. Grievink, F. Kapteijn, J.A. Moulijn, Is a monolithic loop reactor a viable option for Fischer-Tropsch synthesis?, Chem. Eng. Sci., 58 (2003) 583-591.

[6] F. Kapteijn, R.M. de Deugd, J.A. Moulijn, Fischer–Tropsch synthesis using monolithic catalysts, Catal. Today, 105 (2005) 350-356.

[7] C.G. Visconti, E. Tronconi, L. Lietti, G. Groppi, P. Forzatti, C. Cristiani, R. Zennaro, S. Rossini, An experimental investigation of Fischer–Tropsch synthesis over washcoated metallic structured supports, Appl. Catal., A, 370 (2009) 93-101.

[8] R. Güttel, J. Knochen, U. Kunz, M. Kassing, T. Turek, Preparation and Catalytic Evaluation of Cobalt-Based Monolithic and Powder Catalysts for Fischer-Tropsch Synthesis, Ind. Eng. Chem. Res., 47 (2008) 6589-6597.

[9] R. Güttel, C. Eisenbeis, J. Knochen, T. Turek, Monolithic Honeycombs in Loop Reactor Configuration for Intensification of Multiphase Processes, Chem. Eng. Technol., 38 (2015) 1726-1732.

[10] E. Iglesia, S.C. Reyes, R.J. Madon, S.L. Soled, Selectivity Control and Catalyst Design in the Fischer-Tropsch Synthesis: Sites, Pellets, and Reactors, Adv. Catal., 39 (1993) 221-302.

[11] E. Iglesia, S.L. Soled, J.E. Baumgartner, S.C. Reyes, Synthesis and Catalytic Properties of Eggshell Cobalt Catalysts for the Fischer-Tropsch Synthesis, J. Catal., 153 (1995) 108-122.

[12] E. Iglesia, Design, synthesis, and use of cobalt-based Fischer-Tropsch synthesis catalysts, Appl. Catal., A, 161 (1997) 59-78.

[13] L. Fratalocchi, C.G. Visconti, L. Lietti, E. Tronconi, U. Cornaro, S. Rossini, A novel preparation method for "small" eggshell Co/γ-Al2O3 catalysts: A promising catalytic system for compact Fischer–Tropsch reactors, Catal. Today, 246 (2015) 125-132.

[14] A. Jess, C. Kern, Influence of particle size and single-tube diameter on thermal behavior of Fischer-Tropsch reactors: Part II: Eggshell catalysts and optimal reactor performance, Chem. Eng. Technol., 35 (2012) 379-386.

[15] R. Güttel, Structuring of Reactors and Catalysts on Multiple Scales: Potential and Limitations for Fischer-Tropsch Synthesis, Chem. Ing. Tech., 87 (2015) 694-701.

[16] R. Güttel, T. Turek, Improvement of Fischer-Tropsch Synthesis through Structuring on Different Scales, Energy Technol., (2015) submitted.

[17] M. Wolters, L.J.W. van Grotel, T.M. Eggenhuisen, J.R.A. Sietsma, K.P. de Jong, P.E. de Jongh, Combining confinement and NO calcination to arrive at highly dispersed supported nickel and cobalt oxide catalysts with a tunable particle size, Catal. Today, 163 (2010) 27-32.

[18] Ø. Borg, S. Eri, E.A. Blekkan, S. Storsæter, H. Wigum, E. Rytter, A. Holmen, Fischer-Tropsch synthesis over γ-alumina-supported cobalt catalysts: Effect of support variables, J. Catal., 248 (2007) 89-100.

[19] J.P. den Breejen, P.B. Radstake, G.L. Bezemer, J.H. Bitter, V. Frøseth, A. Holmen, K.P.d. Jong, On the Origin of the Cobalt Particle Size Effects in Fischer-Tropsch Catalysis, J. Am. Chem. Soc., 131 (2009) 7197-7203.

[20] J.P. den Breejen, J.R.A. Sietsma, H. Friedrich, J.H. Bitter, K.P. de Jong, Design of supported cobalt catalysts with maximum activity for the Fischer-Tropsch synthesis, J. Catal., 270 (2010) 146-152.

[21] L. Shen, Z. Chen, Critical review of the impact of tortuosity on diffusion, Chem. Eng. Sci., 62 (2007) 3748-3755.

[22] H. Preising, D. Enke, Relations between texture and transport properties in the primary pore system of catalyst supports, Colloids Surf. A, 300 (2007) 21-29.

[23] C.N. Satterfield, C.K. Colton, W.H. Pitcher, Restricted Diffusion in Liquids within Fine Pores, AIChE J., 19 (1973) 628-635.

[24] C.K. Colton, C.N. Satterfield, C.-J. Lai, Diffusion and partitioning of macromolecules within finely porous glass, AIChE J., 21 (1975) 289-298.

[25] S.Y. Lee, J.D. Seader, C.H. Tsai, F.E. Massoth, Restrictive diffusion under catalytic hydroprocessing conditions, Ind. Eng. Chem. Res., 30 (1991) 29-38.

[26] E.M. Renkin, Filtration, Diffusion, and Molecular Sieving through Porous Cellulose Membranes, J. Gen. Physiol., 38 (1954) 225-243.

[27] G. Wang, E. Johannessen, C.R. Kleijn, S.W. de Leeuwa, M.-O. Coppens, Optimizing transport in nanostructured catalysts: A computational study, Chem. Eng. Sci., 62 (2007) 5110-5116.

[28] E. Johannessen, G. Wang, M.-O. Coppens, Optimal distributor networks in porous catalyst pellets. I. Molecular diffusion, Ind. Eng. Chem. Res., 46 (2007) 4245-4256.

[29] S. Gheorghiu, M.-O. Coppens, Optimal bimodal pore networks for heterogeneous catalysis, AIChE J., 50 (2004) 812-820.

[30] M.-O. Coppens, S. Gheorghiu, P. Pfeifer, Optimal design of hierarchically structured nanoporous catalysts, in: S. Abdelhamid, J. Mietek (Eds.) Studies in Surface Science and Catalysis, Elsevier 2005, pp. 371-378.

[31] Y. Zhang, Y. Yoneyama, N. Tsubaki, Simultaneous introduction of chemical and spatial effects via a new bimodal catalyst support preparation method, Chemical Communications, (2002) 1216-1217.

[32] M. Shinoda, Y. Zhang, Y. Yoneyama, K. Hasegawa, N. Tsubaki, New bimodal pore catalysts for Fischer–Tropsch synthesis, Fuel Process. Technol., 86 (2004) 73-85.

[33] B. Xu, Y. Fan, Y. Zhang, N. Tsubaki, Pore diffusion simulation model of bimodal catalyst for Fischer-Tropsch synthesis, AIChE J., 51 (2005) 2068-2076.

[34] P. Munnik, N.A. Krans, P.E. de Jongh, K.P. de Jong, Effects of Drying Conditions on the Synthesis of Co/SiO2 and Co/Al2O3 Fischer–Tropsch Catalysts, ACS Catalysis, 4 (2014) 3219-3226.

[35] T. Witoon, M. Chareonpanich, J. Limtrakul, Effect of bimodal porous silica on particle size and reducibility of cobalt oxide, J Porous Mater, 20 (2013) 481-488.

[36] X.K. Phan, J. Yang, H. Bakhtiary-Davijnay, R. Myrstad, H.J. Venvik, A. Holmen, Studies of Macroporous Structured Alumina Based Cobalt Catalysts for Fischer-Tropsch Synthesis, Catal. Lett., 141 (2011) 1739-1745.

[37] A. Martínez, G. Prieto, J. Rollán, Nanofibrous γ-Al2O3 as support for Co-based Fischer–Tropsch catalysts: Pondering the relevance of diffusional and dispersion effects on catalytic performance, J. Catal., 263 (2009) 292-305.

[38] J. Wang, H. Li, D. Li, J.P. Den Breejen, B. Hou, Influence of the bimodal pore structure on the CO hydrogenation activity and selectivity of cobalt catalysts, RSC Advances, 5 (2015) 65358-65364.

[39] H. Becker, R. Güttel, T. Turek, Optimization of Catalysts for Fischer-Tropsch Synthesis by Introduction of Transport Pores, Chem. Ing. Tech., 86 (2014) 544-549.

[40] H. Becker, R. Güttel, T. Turek, Enhancing internal mass transport in Fischer-Tropsch catalyst layers utilizing transport pores, Catal. Sci. Technol., (2015) accepted.

[41] I.C. Yates, C.N. Satterfield, Intrinsic Kinetics of the Fischer-Tropsch Synthesis on a Cobalt Catalyst, Energy Fuels, 5 (1991) 168-173.

[42] D. Vervloet, F. Kapteijn, J. Nijenhuis, J.R. van Ommen, Fischer-Tropsch reaction-diffusion in a cobalt catalyst particle: aspects of activity and selectivity for a variable chain growth probability, Catal. Sci. Technol., 2 (2012) 1221-1233.

[43] N. Kruse, A.G. Machoke, W. Schwieger, R. Güttel, Nanostructured Encapsulated Catalysts for Combination of Fischer–Tropsch Synthesis and Hydroprocessing, ChemCatChem, 7 (2015) 1018-1022.

[44] J. Knochen, R. Güttel, C. Knobloch, T. Turek, Fischer–Tropsch synthesis in milli-structured fixed-bed reactors: Experimental study and scale-up considerations, Chem. Eng. Process., 49 (2010) 958-964.

[45] R.C. Reuel, C.H. Bartholomew, The stoichiometries of H2 and CO adsorptions on cobalt: Effects of support and preparation, J. Catal., 85 (1984) 63-77.

[46] M.E. Dry, The Fischer-Tropsch process: 1950-2000, Catal. Today, 71 (2002) 227-241.

[47] C. Erkey, J.B. Rodden, A. Akgerman, A correlation for predicting diffusion coefficients in alkanes, Can. J. Chem. Eng., 68 (1990) 661-665.